Modeling Metastable Ion Time-of-Flight Peaks

C. R. Ponciano and E. F. da Silveira*

Departamento de Física, Pontifícia Universidade Católica, C.P. 38071, Rio de Janeiro, RJ 22452-970, Brazil

Received: June 5, 2002; In Final Form: August 1, 2002

An analytical model is presented to describe time-of-flight (TOF) peak shapes of ionized metastable species emitted from solid surfaces under particle or photon bombardment. The model complements and consolidates the formalism for determination of metastable ion mean lives, release energies (*Q*-values), and fragmentation patterns by using linear-type TOF spectrometer data. Effects of fragmentation in the field free region of the TOF spectrometer are discussed. The analysis of phenylalanine TOF spectrum is performed to illustrate the determination of Q and mean life values.

I. Introduction

Time-of-flight (TOF) technique has been used extensively for a long time in Nuclear Physics (e.g., nuclide identification and neutron spectrometry) and mass spectrometry (gas phase samples in particular). In the last 2 decades, the time-of-flight spectrometers conquered new scientific and technologic space, due to the development of solid phase mass spectrometry, especially PDMS[1,2] (plasma desorption mass spectrometry) and MALDI[3,4] (matrix assisted laser desorption ionization). Modern instruments, using electrostatic mirrors,[5] particle ion guides,[6] and delayed extraction electric fields,[7] achieve mass resolving power up to $m/\Delta m \sim 20000$ and a mass range from hydrogen up to molecules as massive as 10^6 u. Combined with a position sensitive ion detector (XY-TOF), this technique can also be employed for electric field mapping[8] and for MS of large gas cells.[9]

Besides TOF applications on mass determination and molecular structure analysis of inorganic, organic, and biological material, a number of surface science phenomena have been studied by using TOF technique, such as secondary electron emission, energy distribution and angular distribution of desorbed ions, spontaneous desorption, ion cluster formation, ion or photon beam interaction with solids, and ion beam material modification. While the TOF analysis of stable ion became routine, the more elaborated metastable ion analysis is much less employed. The basic understanding of the unimolecular decay phenomenon, as well as the development of some associated experimental techniques, was the subject of many researchers in the eighties (e.g., refs 10−16). The main characteristics of metastable ion peaks in mass spectra have been reviewed, for conventional magnetic sector mass analyzers, by Cooks et al.[17] and, for time-of-flight ones in the 1990s, by Schlag[18] and by Cotter.[19] Enlightening articles about cluster dynamics and energy release from metastable decompositions, studied with electrostatic mirror spectrometers, were written by Wei et al.[20] and Barofsky et al.[21] respectively. An alternative method for molecular structure analysis, based on metastable decay, was proposed by Spengler et al.[22,23] under the acronym PSD (post-source decay). In contrast, techniques such as the delayed extraction have been employed to attenuate the undesirable effect of ion metastability that produces tail in mass spectrum peaks (decreasing mass resolving power) and increases background (decreasing mass sensitivity).

The main goal of the present work is to contribute to the theoretical description of desorbed ion unimolecular decay, taking advantage of the time-of-flight technique to determine mean lives of metastable precursors, system kinetic energy increase after fragmentation, and dissociation patterns. In section II and in the Appendix, the basic principles of a unimolecular dissociation model are reviewed and new equations are presented. Only linear-type TOF spectrometer expressions are considered. In section III, the PDMS technique is briefly discussed and PDMS-TOF spectra of phenylalanine are presented. Assuming metastable decay in the field free region, the model predictions are compared with data in section IV. Remember that the yields of metastable ions (including the fragmentation in the acceleration region) emitted in SIMS, PDMS, or MALDI analyses may be comparable or even higher than the stable ones, a fact that must be taken into account by cluster emission models.

II. Time-of-Flight Peak Shape Model

At the time $t = 0$, an energetic projectile or a photon pulse ionizes the target, producing secondary ions which are accelerated toward a zero electric field region. Plume effects may induce either prompt fragmentation or excite molecules to metastable states. The secondary ions or their fragments are detected afterward at distinct time intervals T generating a TOF spectrum. TOF formulas for secondary ions that do not fragment in-flight are well-known (see ref 19, for instance). Whenever an emitted molecule dissociates spontaneously during its free-flight, conservation of the system total energy, total linear momentum, and total charge imposes drastic restrictions on the fragment dynamics.

The frequent and important situation in which the ionized precursor undergoes binary fragmentation, i.e., a unimolecular dissociation leading to formation of a neutral and an ion fragment pair: $m^+ \rightarrow m_0 + m_1^+$, is mainly treated here. Equations for the two fragment times of flight (T^0 and T^+) in linear spectrometers are derived in the Appendix. Definition of parameters is given in Figure 1: the T^+ maximum value (or the T^0 minimum one) is T_m, the nonfragmented precursor TOF; the T^+ minimum value is T_{m1}, the TOF of the fragment ion promptly produced in the sample.

* Corresponding author. E-mail: enio@vdg.fis.puc-rio.br.

10.1021/jp0213405 CCC: $22.00
Published on Web 09/26/2002

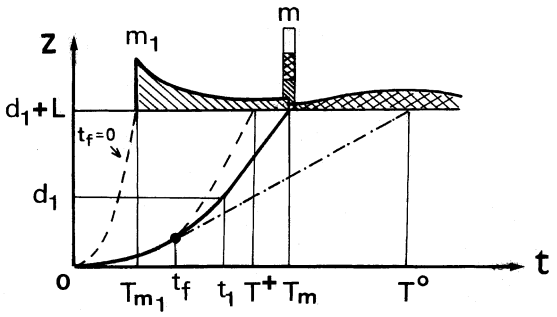

Figure 1. Dependence of the ion precursor (solid line), ion fragment (dash line), and neutral fragment (point dash line) axial coordinates on their time-of-flight. T_m is the precursor TOF if no fragmentation occurs till its arrival at the detector. T_{m1} is ion fragment TOF if prompt fragmentation occurs (the precursor is leaving the sample). In the upper part, a typical TOF spectrum is shown; the broad bump is produced by neutral fragments.

Besides instrumental parameters and the mass of the two fragments, the contribution of metastable ion fragmentation to their time-of-flight spectrum shape depends on

(a) axial component of the initial velocity of the precursor ion (v'_{z0}),

(b) precursor ion mean life τ,

(c) kinetic energy increase after fragmentation Q,

(d) fragmentation branching ratio.

The dependence on the initial velocity has been analyzed for stable ions by many authors (e.g., refs 20−26). Particularly, Pereira et al.[25] have examined how the nuclear and the electronic stopping powers affect the TOF peak shape of desorbed atomic ions.

In the following fragmentation model for metastable spectrum shape analysis, it is assumed: (i) no collisions in-flight, (ii) random and isotropic molecular dissociation, and (iii) the fragmentation probability per time unit is constant. This implies no effect of the acceleration field on the fragmentation process, which could favor emission in the field direction for polar molecules. Therefore if N_0 is the precursor emission yield of a given species, i.e., the average number of metastable ions emitted at the time $t = 0$, the number of survivals per ionization event decreases in time as

$$N(t) = N_0 e^{-t/\tau} \tag{1}$$

and the dissociation rate at a given fragmentation time t_f is

$$n_f(t_f) \equiv -\frac{dN}{dt_f} = \frac{N_0}{\tau} e^{-t_f/\tau} \tag{2}$$

The time-of-flight spectrum shape is given by the variation of detection rate as a function of the time T, elapsed between sample ionization and fragment detection. Considering $Q = 0$, the ion (or neutral) fragments produced by dissociations occurring between t_f and $t_f + dt_f$ reach the detector in the time interval between T and $T + dT$. Moreover, if the detection efficiency ϵ is taken into account, the number of detected ion (or neutral) fragments per impact is given by

$$n(T)dT = \epsilon n_f(t_f)dt_f \tag{3}$$

Consequently, the fragmentation TOF spectrum shape is described by the function:

$$n(T) = \epsilon n_f(t_f)\frac{dt_f}{dT} = \epsilon\frac{N_0}{\tau} e^{-t_f/\tau}\frac{dt_f}{dT} \tag{4}$$

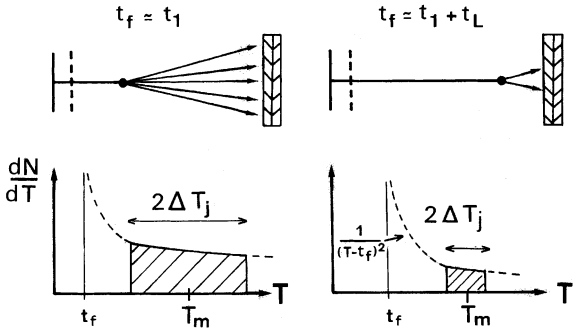

Figure 2. (a) (left) The earlier the fragmentation occurs ($t_f \ll T_m$), the larger is the detector area attainted by the fragments (upper) and broader is the TOF spread (lower). (b) (right) The shortest TOF for a given t_f is $T^{min} \cong T_m - (T_m - t_f)\Delta v/v$. The longest one is $T^{max} \cong T_m + (T_m - t_f)\Delta v/v$. The time spread $2\Delta T = T^{max} - T^{min}$ is large for $t_f \ll T_m$ and small for $t_f \sim T_m$. This mathematical model may be also employed to describe the arrival at a wall of a sound wave produced by a moving source.

To calculate dt_f/dT, the functions $T(t_f)$ for the neutral and the ion fragments are needed. These expressions are deduced in the Appendix. Remember that for $Q = 0$ process occurring in the field-free region ($t_1 < t_f < T_m$), the fragments have the precursor ion velocity and, consequently, the same TOF (eq A1). The fact that, for fragmentation in this region, T does not vary while t_f increases implies that dt_f/dT diverges in eq 4, generating a sharp peak at time T_m in the TOF spectrum.

If $Q > 0$, the peak at T_m spreads out, due to the existence of different axial velocities for each fragment ($m_0\Delta v_0 = m_1\Delta v_1$, eq A3). As illustrated in Figure 2, this spread is maximum if $t_f \cong t_1$ and vanishes if $t_f \to T_m$. The neutral and ion fragment TOF peaks have then the shape given by eq A9.

For metastable decays in which $Q \ll qU$ and $\tau > T_m$:

$$n(T) \cong \frac{N_0}{T_m}(1 - e^{-T_m/\tau})\left[\frac{1}{2}\ln\left(\frac{m_1}{m_0}\frac{Q}{qU}\right) - \ln\left|\frac{T - T_m}{T_m}\right|\right] \tag{5}$$

This expression suggests that $n(T) \times \ln|\Delta T|$ plot is a convenient method to extract the Q-value from experimental data. An experimental difficulty exists when $m_1 \ll m_0$, in which case the ion fragment has relatively low kinetic energy and its detection efficiency may be close to zero. One possible issue is to analyze fragmentation (of the same species) occurring in the acceleration region, which allows the ion fragment to increase its energy.

III. Experimental Section

Secondary ions were produced by the ^{252}Cf fission fragments impacting on target surface. In each event, the complementary fission fragment gives the start signal for TOF measurement. Figure 3 presents a sketch of the PDMS spectrometer employed. Details of the ^{252}Cf−PDMS technique are described by Macfarlane.[1,2,19] Time-of-flight spectra of Phenylalanine (Phe) positive ions were obtained with a spectrometer having respectively $d_1 = 0.70$ cm and $L = 134.45$ cm lengths of acceleration and field-free regions. The targets were prepared by sample evaporation in a vacuum onto thin Al foils. Acceleration potentials were $U = 3.5$ and 15 kV, to change precursor ion velocities of about a factor 2 and, consequently, to change the ratio τ/t_1 by the same factor. Two grids (not shown in the figure), close and parallel to the secondary particle detector, could be biased (zero potential at the first grid and U_G at the second one) to create a deceleration region for ions. According to the retarding potential U_G, ion fragment detection can be partially

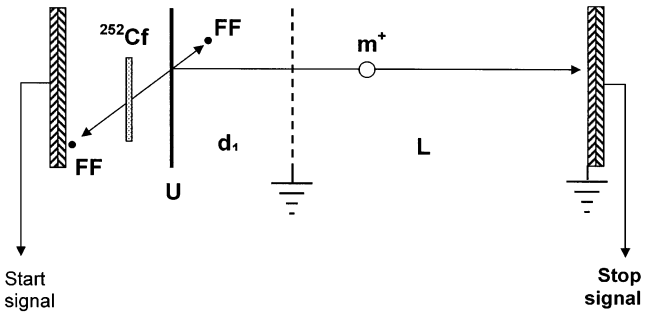

Figure 3. Sketch of the PDMS spectrometer, in transmission mode. The ^{252}Cf fission fragment traverses a thin target (biased at U), inducing ion desorption. The ion (mass m, charge q) is accelerated by an electric field U/d_1 toward the free field region of length L. The TOF is given by the time interval between the start and stop signals and is proportional to $\sqrt{m/q}$.

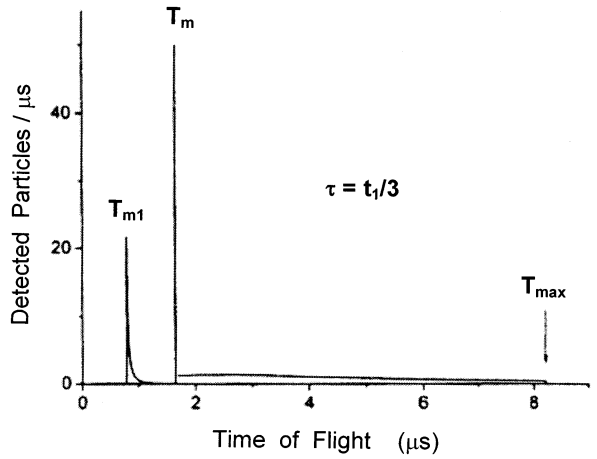

Figure 4. Predicted TOF spectrum shape for a metastable fragmentation $130^+ \rightarrow 100^+ + 30°$, $t_1 = 150$ ns, and $\tau = 50$ ns. The spectrometer parameters used in the simulation are $d_1 = 1.0$ cm, $L = 100$ cm, and $U = 12$ kV. At $T = T_{max}$, data acquisition is supposed to stop. T_m and T_{m1} are the precursor peak and the prompt ion fragment peak times of flight, respectively.

($U_G < U$) or totally ($U_G > U$) eliminated. This ion filter setup is convenient for simplifying the peak analysis of the neutral fragments formed in the field-free region.

IV. Results and Discussion

Depending whether the precursor half-life (τ ln 2) is smaller or greater than t_1, most of the fragmentation events occur in the acceleration region or in the field-free region. If fragmentation occurs in acceleration region, neutral fragments have average velocities lower than those of the ion fragments which have their acceleration increased after dissociation, as shown in the Figure 4. This fact reduces enormously (or completely) the spectrum background at lower mass region due to neutrals: an "ion tail" appears at the right side of each ion fragment peak, decreasing up to the precursor peak (Figures 1 and 2); the "neutral tail" appears at right side of each precursor peak. If fragmentation occurs in the field-free region, neutral and ion fragments have the same average velocity and quasi-symmetrical tails appear at both sides of each precursor ion peak. Some model predictions for fragmentation in the field-free region are discussed below.

Figure 5 shows the amino acid phenylalanine mass spectra obtained at $U = 15$ kV for retarding field "on" (upper) and "off" (lower). In the first one, three phenylalanine characteristic peaks correspond to neutrals fragments produced by unimo-

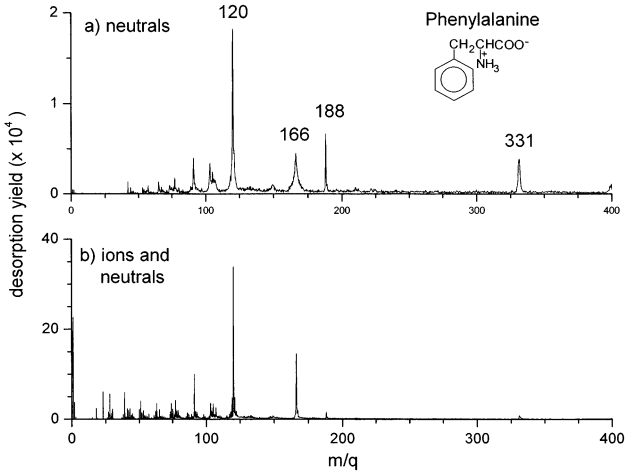

Figure 5. Phenylalanine PDMS spectra, obtained with 15 kV of acceleration potential: (4a) the retarding field is "on" with $U_G = 17.6$ kV: only neutrals are detected; (4b) ion and neutrals are detected, since this field is "off".

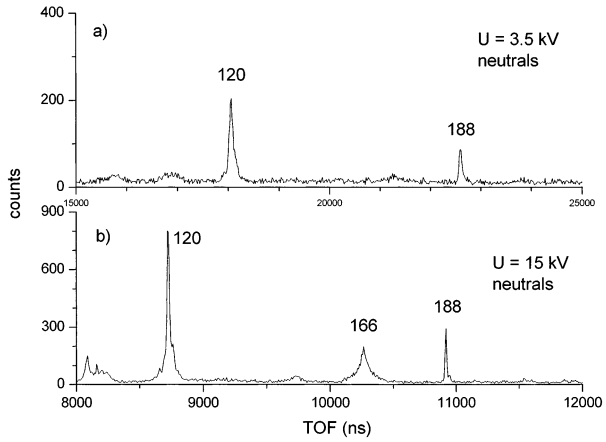

Figure 6. Phenylalanine PDMS TOF-spectra of neutrals, obtained for two different acceleration and retarding potentials: (a) $U = 3.5$ kV and $U_G = 4.1$ kV; (b) $U = 15$ kV and $U_G = 17.6$ kV. The 166^+ ions are slower in the 3.5 kV case and have decayed almost completely in the acceleration region.

lecular fragmentation in the drift region of precursor ions of masses 166, 331, and 120 u, respectively, due to the species $[Phe + H]^+$, $[2Phe + H]^+$ (protonated dimmer), and $C_8H_{10}N^+$ (the fragment ion produced by the $[Phe + H]^+ \rightarrow C_8H_{10}N^+ + HCOOH^0$ decay). The second spectrum (Figure 5b) has more complex peaks, because all the desorbed ion species are included, and illustrates the convenience of using only the neutral spectrum for peak shape analysis: remember that the dissociation in the field-free region implies that all fragments of a given precursor have their TOF centered at the corresponding T_m. Note also that the spectrometer TOF resolution is revealed by the stable ion peaks, so the broad peaks indicate metastable species.

Figure 6 presents part of the neutral fragment TOF spectrum for two acceleration potentials: $U = 3.5$ kV (upper) and for $U = 15$ kV (lower). Note in particular that in the 3.5 kV spectrum the 166 u mass peak is strongly attenuated with respect to 188 u mass peak, both ion species being detected with same efficiency for a given acceleration potential. As the 166 u mass peak disappears in the $U = 3.5$ kV spectrum, an upper limit of $T_m \approx 20$ μs for its mean life may be estimated. Assuming the $166^+ \rightarrow 120^+ + 46°$ fragmentation, $Q = 1.5$ eV, and $\tau = 10$ μs can be determined, by using eq 10 applied for the $U = 15$ kV spectrum data.

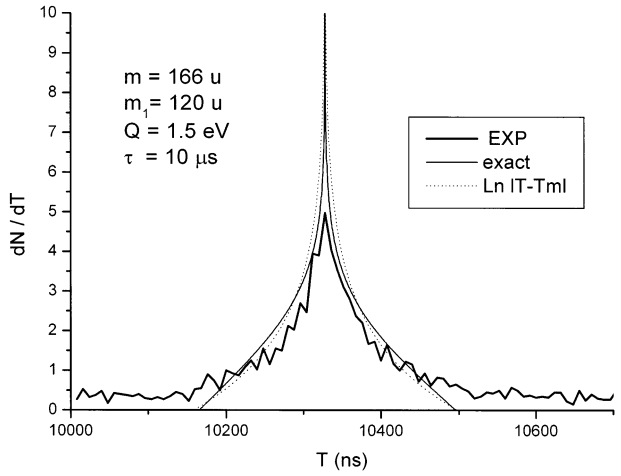

Figure 7. TOF-spectrum of the neutral fragment of mass 166 u quasi molecular ion $[M + H]^+$. Its cuspid-shape peak (Eiffel Tower-like) is characteristic of metastable species. The thick solid line corresponds to experimental data (same phenylalanine spectrum of Figure 5b). The thin solid and the dash line are the model predictions for the $166^+ \rightarrow 120^+ + 46°$ fragmentation. The values $Q = 1.5$ eV and $\tau = 10$ μs are obtained using eqs A10 and A9, respectively.

Figure 7 presents the comparison of measured and calculated TOF neutral fragment peak shapes: solid and dot lines correspond respectively to predictions given by "exact" numerical calculation (eq A9) and by logarithm approximation (eq A10). The theoretical results are overestimated in the central region of the peak for two reasons: (i) TOF instrumental resolution was neglected in the calculation, (ii) the distance between the ion filter and the detector was considered zero. Among the possible decay pathways, $m_1 = 120$ u was preferred because it was reported[27] that the dissociation $166^+ \rightarrow 120^+ + 46°$ is much more likely than the $166^+ \rightarrow 149^+ + 17°$ one.

V. Conclusion

An analytical model for binary fragmentation is presented and applied for metastable ions emitted from bombarded solid surfaces and dissociating in a field-free region. The model is designed for linear TOF spectrometers, but it may be extended to Reflectrons or other TOF instruments. An expressive feature of the model is its ability to provide a direct connection between TOF peak shapes with the dynamics of the flying ions. As a consequence, it is possible to parametrize time peaks in terms of ion masses, absolute desorption yields, emission (initial) velocities, mean lives, *Q*-values, and branching ratios, which are relevant data for microscopic models concerning molecular fragmentation and solid relaxation. As an illustrative example, model predictions are compared with experimental time-of-flight measurements of phenylalanine samples, providing good agreements and determination of Q and τ.

Acknowledgment. CNPq, PADCT III and FAPERJ are acknowledged for their partial financial support.

Appendix

Time-of-Flight for the Ion and Neutral Fragments. A linear time-of-flight spectrometer is formed by an acceleration region and by a field free region with lengths d_1 and L, respectively (see Figure 3). U is the acceleration potential. Many authors have shown (see Cotter's review,[19] for instance) that the time-of-flight of a stable ion, emitted with initial energy $qU_z \cong 0$, is the sum $t_1 + t_L$ of the TOFs in each region:

$$T_m = t_1 + t_L = 2276.4\sqrt{\frac{m(u)}{q(e)U(kV)}}\left[\frac{2d_1}{\sqrt{U_z/U} + \sqrt{1 + U_z/U}} + \frac{L}{\sqrt{1 + U_z/U}}\right] \cong t_1\left(1 + \frac{L}{2d_1}\right) \quad \text{(A1)}$$

T_m is given in nanoseconds; L and d_1 are given in meters. The mass m is expressed in atomic mass units (1 u = 1.66054402 $\times$ 10^{-27} kg).

If $Q = 0$ fragmentation $m^+ \rightarrow m_0 + m_1{}^+$ occurs at $t_f \geq t_1$, i.e., in the field-free region, both ion and neutral fragments will be detected at the same time. Their TOF is equal to the precursor one if no fragmentation occurs: $T^0 = T^+ = T_m \approx t_1(1 + L/2d_1)$.

Evaluation of *Q* from the Time-of-Flight Spread. Whenever the dissociation $m^+ \rightarrow m_0 + m_1{}^+$ takes place, the total kinetic energy increases by the amount:

$$Q = \Delta E_k = \left(\frac{1}{2}m_0 v_0{}^2 + \frac{1}{2}m_1 v_1{}^2\right) - \left(\frac{1}{2}m v^2\right) \quad \text{(A2)}$$

As the total linear momentum must remain constant, the increase of the neutral and ion fragment velocities can be determined:

$$\Delta v_0 = \sqrt{\frac{2m_1}{mm_0}Q} \qquad \Delta v_1 = \sqrt{\frac{2m_0}{mm_1}Q} \quad \text{(A3)}$$

If θ is the neutral fragment angle of emission, with respect to the precursor velocity, the axial velocities of both fragments are

$$v_{0z} = v + \Delta v_0 \cos\theta \quad v_{1z} = v + \Delta v_1 \cos(\pi + \theta) \quad \text{(A4)}$$

For dissociation at the time t_f in the field-free region, i.e., $t_1 \leq t_f \leq T_m$, the times of flight for the two fragments T^0 and T^+ are given by

$$T = t_f + \frac{L - v(t_f - t_1)}{v + \Delta v \cos\theta} = \frac{T_m + t_f\frac{\Delta v}{v}\cos\theta}{1 + \frac{\Delta v}{v}\cos\theta} \quad \text{(A5)}$$

where $T = T^0$ and $T = T^+$ correspond to $\cos\theta$ and $\cos(\theta + \pi)$ emission, respectively. As usually $Q \ll qU$, one has $\Delta v \ll v$. Then,

$$\Delta T \equiv T_m - T = \frac{\Delta v}{v}(T_m - t_f)\cos\theta \quad \text{(A6)}$$

For a given t_f, the largest TOF spread $\Delta T = |T - T_m|$ will occur for the time interval corresponding to emissions at $\theta = 0$ or at $\theta = \pi$. Considering both $t_L \gg t_1$ (i.e., the usual spectrometer geometry $L \gg d_1$; $v \cong L/T_m$) and $t_f \cong 0$ (the highest fragmentation rate), the maximum ΔT value, ΔT_{max}, is obtained. So that, $\Delta v = L\Delta T_{max}/T_m{}^2$. The total spread at the peak is $2\Delta T_{max}$. Making use of eq A3, Q may be then evaluated. For neutrals,

$$Q \cong \frac{m_0}{m_1}qU\left(\frac{\Delta T_{max}{}^0}{T_m}\right)^2 = 2\frac{m_0 q^2}{m_1 m L^2}(U\Delta T_{max}{}^0)^2 \quad \text{(A7)}$$

which shows, for a given spectrometer, that the product $U\Delta T_{max}$ should be constant for each desorbed metastable species. As $T_m\sqrt{U}$ is constant (eq A1), one has that $\Delta T_{max}/T_m \propto 1/\sqrt{U}$

which means that the metastable TOF spread is relatively more accentuated at low acceleration potentials.

TOF Peak Shape Dependence on *Q*. If a large number of molecular fragmentations occurs isotropically in the field-free region, the neutral and ion fragments produced between t_f and $t_f + dt_f$ should be randomly dispersed in two concentric spherical shell layers of radii R_0 and R_1. The sphere center moves toward the detector with the precursor velocity v, while each radius R increases with the corresponding velocity $\Delta v \ll v$ given by eq A3. The layer thickness is $\Delta v\, dt_f$.

In these $\Delta v\, dt_f$ thick layers, the number of fragments in a solid angle $d\Omega$ is constant and equal to $d(dN/dt_f) = (d\Omega/4\pi)\, n_f(t_f)$. During the time interval between T and $T + dT$, all the fragments inside the shell and laying in a ring defined by the solid angle $d\Omega = 2\pi \sin\theta\, d\theta$ are detected at the rate

$$\frac{d^2N}{dT\, dt_f} = \frac{1}{4\pi} n_f(t_f) 2\pi \sin\theta \frac{d\theta}{dT} = \frac{n(t_f)}{2} \frac{v}{\Delta v} \frac{T_m - t_f}{(T - t_f)^2} \quad \text{(A8)}$$

where θ is the emission angle in the precursor frame and the dependence of $\sin\theta\, d\theta = -d(\cos\theta)$ on T is given by eq A5. This result is sketched in Figure 2 for two different values of the fragmentation time t_f. For t_f close to zero (or to t_1), the fragmentation rate is high (see eq 2) but the fragment arrival time is very spread ($2\Delta T \cong 2T_m \Delta v/v$, eq A6). Inversely, for $t_f \cong T_m$, the fragmentation rate is lower but impact rate is the highest since $\Delta T \to 0$. Finally, using eq 2, the spectrum shape is obtained by integrating this function over a t_f range which allows detection at time T; that is, from t_1 to $t_f^{max} = T - |T - T_m| v/\Delta v$:

$$n(T) \equiv \frac{dN}{dT} = \frac{v}{2\Delta v} \frac{N_0}{\tau} \int_{t_1}^{t_f^{max}} e^{-t_f/\tau} \frac{T_m - t_f}{(T - t_f)^2} dt_f \quad \text{(A9)}$$

where $t_f^{max}(T)$ is the latest fragmentation time compatible with detection at $t = T$ (see Figure 4b). A discussion on peak shapes, based on this expression, can be found in ref 28.

The following comments are relevant at this point:

(i) For the spectrometers having retarding potential device, t_f^{max} must be limited to the value $t_1 + t_R$, where t_R is the TOF in the new field free region.

(ii) A slightly asymmetric peak shape is predicted, its maximum being at T_m. If $\tau \ll t_1$, fragmentation occur essentially close to the sample, no precursor peak shows up and the ion fragment peak has a tail to the left (toward shorter times), similarly to emissions with nonzero initial energies U_z. If $\tau \geq T_m$, the exponential factor in eq A9 may be approximated by its mean value over the time interval T_m and analytical integration can be carried out. To avoid lengthy expressions, only the case of interest $\Delta v \ll v$ is considered below. Then,

$$n(T) = \frac{N_0}{T_m}(1 - e^{-T_m/\tau}) \ln \frac{T_{max} - T_m}{|T - T_m|} \quad \text{(A10)}$$

(iii) The function $\ln(\Delta T_{max}/\Delta T)$ decreases from infinity to zero when ΔT varies from zero to ΔT_{max}, the logarithmic divergence at $T = T_m$ disappearing for experimental data. If δT is the time resolution of equipment, one should replace the function $n(T)$ by its average over each δT interval. At $T = T_m$:

$$\overline{n(T)} = \frac{1}{\delta T} \int_{T_m - (\delta T/2)}^{T_m + (\delta T/2)} n(T)\, dT = \frac{N_0}{T_m}(1 - e^{-T_m/\tau}) \left(1 + \ln \frac{T_{max} - T_m}{\delta T/2}\right) \quad \text{(A11)}$$

(iv) A peak deformation close to its maximum may appear due the finiteness of the detector radius ρ: the fragments emitted perpendicularly to the precursor velocity may not be detected. The condition for detection is $\Delta v \sin\theta (T_m - t_f) \leq \rho$, which becomes more restrictive for small t_f (i.e., the largest $T_m - t_f$), precisely when the fragmentation rate is the highest.

References and Notes

(1) Macfarlane, R. D.; Torgenson, D. F. *Science* **1976**, *191*, 920.
(2) Macfarlane, R. D. Methods in Enzymology. In *Mass Spectrometry*; McCloskey, A. J., Ed.; 1990; Vol. 193, p 263.
(3) Tanaka, K.; Ido, Y.; Akita, S. *Mass Spectroscopy*; Matsuda, H., Liang, X. T., Eds.; Bando Press: Osaka, 1987; p 185.
(4) Karas, M.; Bachmann, D.; Bahr, U.; Hillenkamp, F. *Int J. Mass Spectrom. Ion Processes* **1987**, *78*, 53.
(5) Mamyrin, B. A.; Karataev, V. I.; Schikk, D. V.; Zagulin, V. A. *Sov. Phys. JETP* **1973**, *37*, 45.
(6) Davis, K. V.; da Silveira, E. F.; Schweikert, E. A. *Nucl. Instrum. Methods* **1988**, *A273*, 203.
(7) Vestal, M.; Juhasz, P. *J. Am. Soc. Mass Spectrosc.* 1998, 893.
(8) Jalowy, T.; Neugebauer, R.; Groeneveld, K.; Ponciano, C. R.; Farenzena, L. S.; da Silveira, E. F. *Rev. Sci. Instrum.* **2002**, *73*, 3187.
(9) Jalowy, T.; Neugebauer, R.; Groeneveld, K.; Ponciano, C. R.; Farenzena, L. S.; da Silveira, E. F. *Int. J. Mass Spectrom.* **2002**, *219*, 343.
(10) Chait, B. T.; Field, F. H. *Int. J. Mass Spectrom.* **1981**, *41*, 17.
(11) Kühlewind, H. *Int. J. Mass Spectrom.* **1983**, *51*, 255.
(12) Chait, B. T. *Int. J. Mass Spectrom.* **1983**, *53*, 227.
(13) Chait, B. T.; Field, F. H. *J. Am. Chem. Soc.* **1984**, *106*, 1931.
(14) Della-Negra, S.; Le Beyec, Y. *Anal. Chem.* **1985**, *57*, 57.
(15) Neusser, H. J. *Int. J. Mass Spectrom Ion Processes* **1987**, *79*, 141.
(16) Tang, X.; Beavis, R.; Ens, W.; Lafortune, F.; Schueler, B.; Standing, K. G. *Int. J. Mass Spectrom. Ion Processes* **1988**, *85*, 43.
(17) Cooks, R. G.; Beynon, J. H.; Caprioli, R. M.; Lester, G. R. *Metastable Ions*; Elsevier Science Publishing Co.: New York, 1973.
(18) Schlag, E. W., Ed. Time-of-Flight Mass Spectrometry and its Applications. In *International Journal of Mass Spectrometry and Ion Processes*; Elsevier: New York, 1994; p 131.
(19) Cotter, R. J., Ed. *Time-of-Flight Mass Spectrometry: Instrumentation and Applications in Biological Research*; ACS Professional Reference Books; American Chemical Society: Washington, DC, 1997.
(20) Wei, S.; Castleman, A. W., Jr. *Int. J. Mass Spectrom. Ion Processes* **1994**, *131*, 233.
(21) Barofsky, D. F.; Brinkmalm, G.; Håkansson, P.; Sundqvist, B. U. R. *Int. J. Mass Spectrom. Ion Processes* **1994**, *131*, 283.
(22) Spengler, B.; Kirch, D.; Kaufmann, R. *J. Phys. Chem.* **1992**, *96*, 9678. Spengler, B. *Protein and Peptide Analysis by Mass Spectrometry*; John Chapman, R. J., Ed.; Humana Press, Inc.: Totowa, NJ, 1996.
(23) Spengler, B. *J. Mass Spectrom.* **1997**, *32*, 1019.
(24) de Castro, C. C.; Bitensky, I. S.; da Silveira, E. F.; Most, M.; Wien, K. *Int. J. Mass Spectrom. Ion Processes* **1998**, *173*, 1.
(25) Pereira, J. A. M.; da Silveira, E. F. *Phys. Rev. Lett.* **2000**, *84*, 5904.
(26) Wang, G. *Nucl. Instrum. Methods Phys. Res.* **1988**, *B33*, 502.
(27) Ponciano, C. R. Ph.D. Thesis, Pontifícia Universidade Católica, Rio de Janeiro, Brazil, 1996.
(28) Ponciano, C. R.; Ladeia, R, C. C.; Collado, V. M.; da Silveira, E. F. *Braz. J. Phys.* **2001**, *31*, 514.